

Point Spread Function Reconstruction in PET

Michael E. Casey, Ph.D, Director of Physics, Siemens Molecular Imaging

www.siemens.com/mi

SIEMENS
medical

Introduction

A major improvement in PET image quality was reached with the introduction of iterative reconstruction in the 1990's. While researchers had studied the techniques for many years, three innovations made iterative reconstruction practical in clinical application. First was the discovery of the ordered subset method, which increases the convergence rate of the expectation maximization (OSEM) algorithm. The second was the discovery of the Fourier rebinning algorithm that converts a three dimensional reconstruction into a two dimensional problem, allowing 2D OSEM to be used and thus, making the overall reconstruction faster. The third was the continued improvement in the speed of available computers, making the reconstruction available in reasonable time. Now as computers have further increased in speed, the image quality can be improved by removing more of the approximations incorporated in the algorithms.

Basics of iterative reconstruction

Positron emission tomographs do not measure an image directly. Instead, they measure a sinogram that consists of an array of the sums of all the counts along the lines connecting two detectors. The problem is how to turn this measurement into an image.

The expectation maximization (EM) algorithm solves the problem in the following way. First, the algorithm assumes an image. This initial image is usually uniform (all the voxels are the same value – typically ones.) Then using a model of the detection process, the algorithm simulates (forward projects) the sinogram

from the assumed image. This step involves adding up the counts from all the voxels along the lines of response (LORs). The resulting sinogram is, of course, different from the measured sinogram so the algorithm finds the differences and updates the assumed image (back projects) to form a new estimate. The loop is repeated with the estimated image becoming closer and closer to the true image with each circuit through the loop. In mathematical notation, the EM algorithm can be expressed as:

$$i_j^{k+1} = i_j^k \cdot \frac{1}{\sum_i p_{i,j}} \sum_i \left[p_{i,j} \cdot \frac{s_i}{\sum_j p_{i,j} \cdot i_j^k} \right]$$

Equation 1.

Here, the sinogram is denoted by the symbol s and the image by i . The probability that sinogram bin i contributes to image voxel j is contained in the matrix p . The fraction term in Equation 1 is the error between the measured sinogram and the simulated sinogram (denominator). If the measured and simulated sinogram match, the error term (last term in the equation) is unity and does not change the image.

Ordered Subset

An LOR is the imaginary line connecting two detectors. The measurement – the sinogram – consists of an array of the counts from the detector pairs. Typically, the sinogram is ordered so that a set of parallel LORs occupies one row of the sinogram. Each successive row contains LORs that are parallel but at a slightly different angle than the previous row.

Ordered subset EM reconstruction follows the basic flow as described in the above paragraph with the one extension of using only a subset of all the rows in the sinogram to update the image. One iteration occurs when all possible subsets are used. For example, if the sinogram consists of 128 rows or angles, one might choose to use 16 subsets. Each subset will consist of 16 angles. The first subset could be rows 0, 16, 32, etc. The next subset will be rows 8, 24, 40, etc. By using the ordered subset approach, the estimated image approaches the true image faster. The increase in speed occurs because there is less computation required for a subset of the rows as compared to using all the rows. The increase in speed over the EM algorithm can be estimated from the fact that the product of the number of iterations and the number of subsets is about constant for equivalent images. So for 16 subsets, the image is formed 16 times faster.

Statistical Data

The data in the sinogram bins consists of the counts along the LORs. Since the counts come from nuclear decay, they occur randomly. The number of counts that is collected in a sinogram bin is governed by a Poisson process. This means that the uncertainty or standard deviation of the number of counts collected in a bin follows the square root of the number. The derivation of the expectation maximization algorithm starts with the assumption of Poisson statistics.

Including corrections

The above description assumes that the data are perfect. In reality, they are not. Several physical effects distort the measurement and thus, require correction in order to be able to produce accurate images. The distortions are due to random coincidences, non-uniform detector response, attenuation, scattered radiation and scanner geometry.

Originally, the sinogram was corrected for the physical distortions and then Equation 1 was used to produce the image. However, the corrections distort the Poisson nature of the data and can confuse the algorithm, producing less ideal images. This occurs because the algorithm weights the data based on the uncertainty. Data with higher uncertainty receives less weight than data with lower uncertainty. If the weights applied do not match the uncertainty in the data, the image noise will not be optimal.

One simple step toward a more realistic weighting was the introduction of attenuation weighted OSEM (AW-OSEM). In AW-OSEM algorithm, the attenuation was included in the p matrix of Equation 1. Recall that the p matrix contains the probability that an emission from image voxel j is detected in sinogram bin i .

Corrections to the data such as randoms and scatter require a subtraction and can produce negative values in the sinogram. Since physically there is no such thing as a negative count, these values are arbitrarily truncated to zero. This also has the effect of confusing the algorithm and compromising image quality.

Since the aim of the iterative reconstruction is to recover the image that most likely produced the measurement, the simulation of the sinogram from a given image must be accurate. This can be accomplished by adding in the scatter and randoms to the simulated sinogram and simulating the effects of attenuation and non-uniform detector response. The resulting equation is then:

In this Equation 2, the randoms, r_i , and the scatter, c_i , are added to the simulated (forward projected) sinogram. The normalization, n_i , which corrects for non-uniform detector response and the attenuation, a_i , are combined with the probability matrix, $p_{i,j}$ to allow the correct weighting. Since the simulated sinogram does not have the effects of non-uniform response and attenuation, these effects are created in the randoms and scatter by the multiplication.

Including detector spatial response

While Equation 2 properly treats the corrections, it does not necessarily handle the spatial response of the detector system. As stated earlier, the $p_{i,j}$ matrix contains the probability that an event emitted from an image voxel j is counted in sinogram bin i . If the sinogram bins are equally spaced radially, the naïve and simple approach is to use the trigonometric translation from the image to the sinogram and to interpolate between two sinogram bins. This is the approach com-

$$i_j^{k+1} = i_j^k \cdot \frac{1}{\sum_i \left(p_{i,j} \cdot \frac{1}{n_i \cdot a_i} \right)} \cdot \sum_i \left[p_{i,j} \cdot \frac{s_i}{\left(\sum_j p_{i,j} \cdot i_j^k \right) + a_i \cdot (r_i \cdot n_i + c_i)} \right]$$

Equation 2.

monly used in filtered back projection in most imaging modalities. However, if the goal is an accurate representation of the probability that an image voxel is counted in the sinogram bin, the naïve approach can produce less than optimum results.

The PET scanner consists of a circular ring of detectors. This geometry introduces two distortions into the detection process. One distortion occurs when the LORs are grouped into parallel sets; the distance between LORs in the radial direction is not uniform. The distance between lines narrows with increasing distance from the center of the tomograph. The second distortion is caused by the increasing tilt of the crystals. As the crystal tilts in LORs off center, the point response gets broader. This effect is illustrated in Figure 1.

The problem of the non-linear sampling can be easily compensated for in the algorithm. In the AW-OSEM and in filtered back projection, this was done by interpolating the rows of the sinogram to produce evenly spaced samples. However, to preserve the Poisson statistics, the algorithm must compensate for the non-linear sampling in the measurement estimation and in the update of the estimated image.

The effect of the tilting crystals is another matter. To compensate for this effect, the shapes of the point spread response are stored and used during the measurement estimation step of the algorithm. The point spread functions can be viewed as the probability that an event in an image voxel contributes to a sinogram bin. This probability dictates that an event emitted from a single image voxel might be recorded in any of a number of sinogram bins.

The precise matching of the point spread functions in the reconstruction has the effect of reducing the high frequency noise in the image, simultaneously improving the spatial resolution of the image. Both effects occur since the point spread functions act much like a matched filter, enhancing the data that matches the detection model and rejecting the noise that does not match. Precise matching is important. If the point spread function is too narrow, such as that assumed in AW-OSEM, then the data dominates the spatial resolution. If the point spread function is too broad, then ringing occurs where image intensities change. Therefore, in the PSF reconstruction, the point spread functions change shape with each sinogram bin.

To insure precise matching of the point spread functions (PSF), they were measured using a point source placed at many positions in the field of view. To produce point spread functions with sampling small enough to be used in a reconstruction algorithm, the measurements were fit with a function representation.

Phantom Studies

The usually accepted measure of spatial resolution is to measure point sources suspended in air. Measurements were taken at radial positions from the center to 28 centimeters in 4 centimeter steps. The data were reconstructed with a standard filtered backprojection algorithm using FORE rebinning and with the PSF algorithm using six iterations and 14 subsets. The matching of the point spread functions allows the PSF algorithm to recover resolution up to the Nyquist limit and to produce relatively uniform resolution to the edge of the field of view. This data is illustrated in Figure 2.

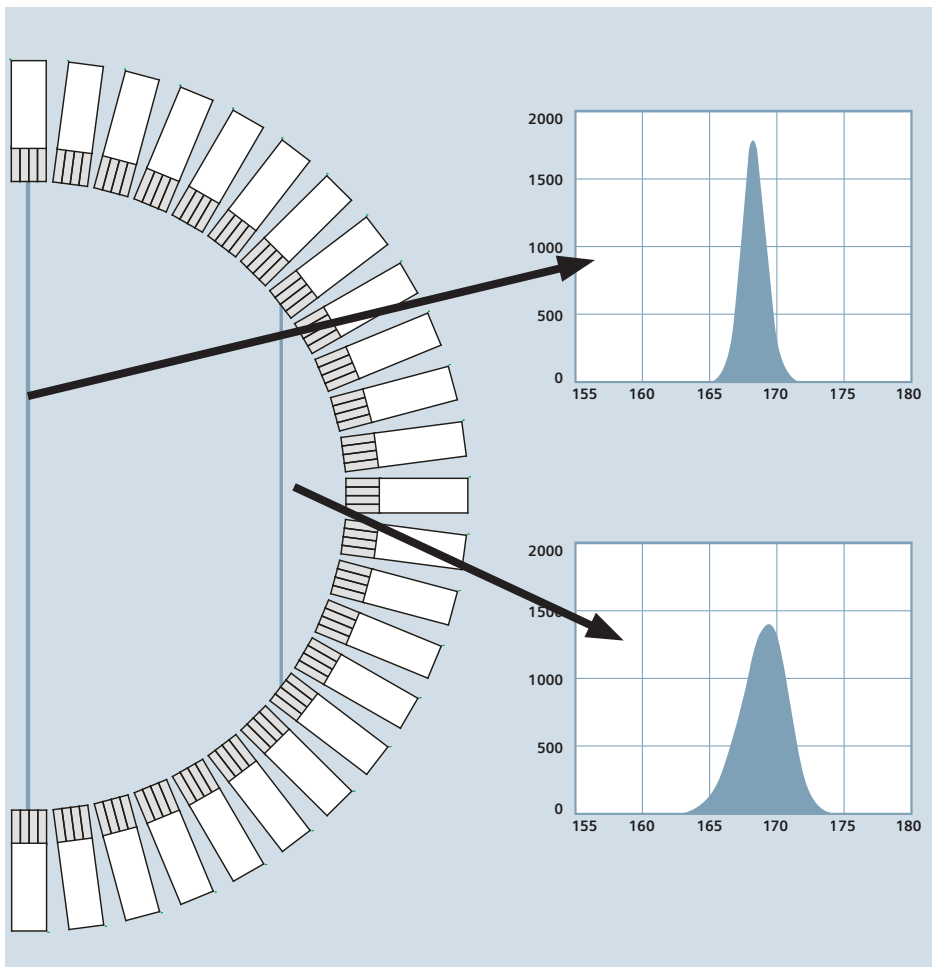


Figure 1.

Illustration showing the non-linear spacing in parallel lines of response and the broadening of the point spread function with increasing detector tilt.

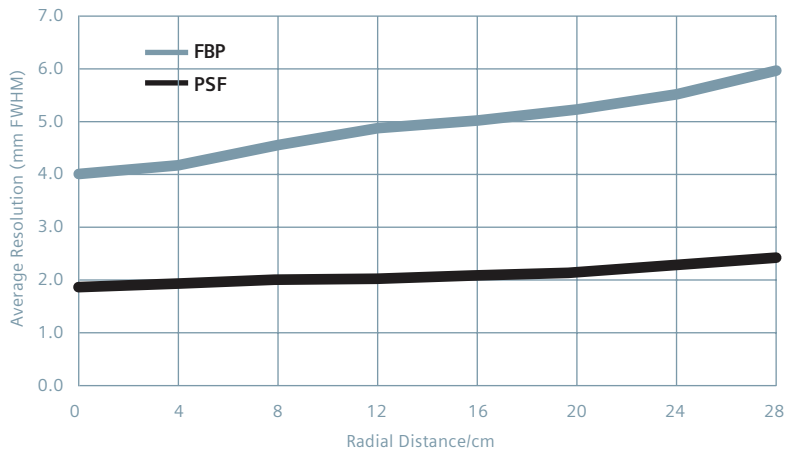


Figure 2. Average of radial and tangential resolution measured using a line source.

While the superb resolution achieved by imaging a point source in air is impressive, a more clinically relevant task is to image hot lesions in a warm background. The following phantom experiment illustrates that uniform recovery can be achieved in a more realistic imaging situation. An Anthropomorphic Torso Phantom (Data Spectrum Corp) was modified to include four twelve millimeter silicon spheres impregnated with 38 microCuries of ^{68}Ge suspended in the background. The background portion of the phantom was filled with ^{18}F and the liver filled with twice that concentration. Data was acquired for 2 hours. The resulting data was reconstructed by both AW-OSEM and PSF with 6 iterations and 14 subsets. The resulting images were filtered with a 4 mm 3D Gaussian filter. These images are shown in Figure 3.

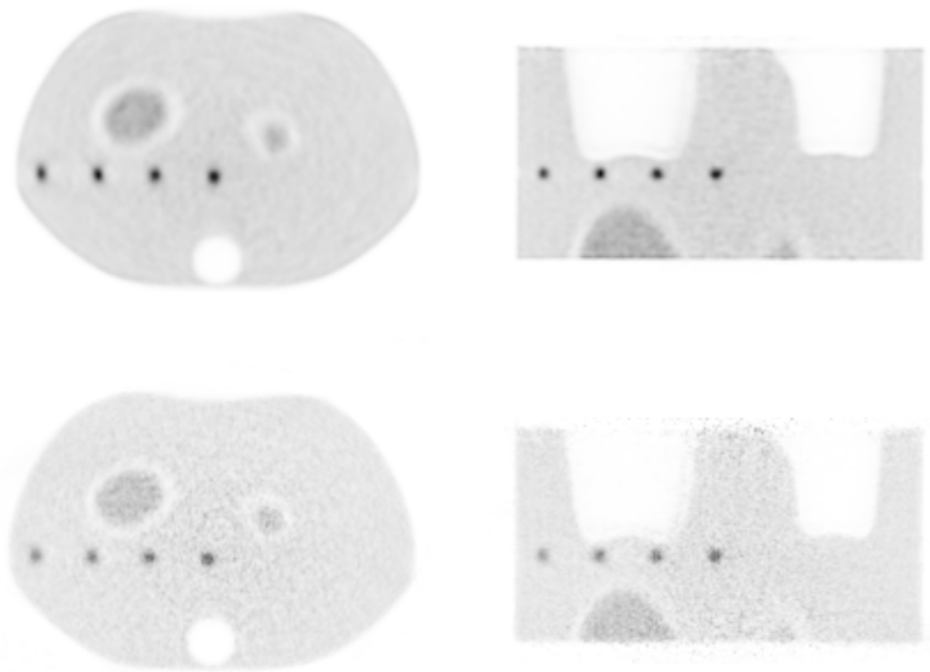


Figure 3. The Anthropomorphic Torso Phantom with the silicon spheres used in the recovery experiment. Upper: PSF reconstruction. Lower: AW-OSEM.

To assess the recovery, volumes of interest were drawn on the spheres that included all pixels within three pixels of the peak value. The region of interest (ROI) values were normalized to the background. These ROI values are shown in the chart in Figure 4. Notice how the AW-OSEM ROI values decrease with increasing distance from the center while the PSF values exhibit more consistent recovery.

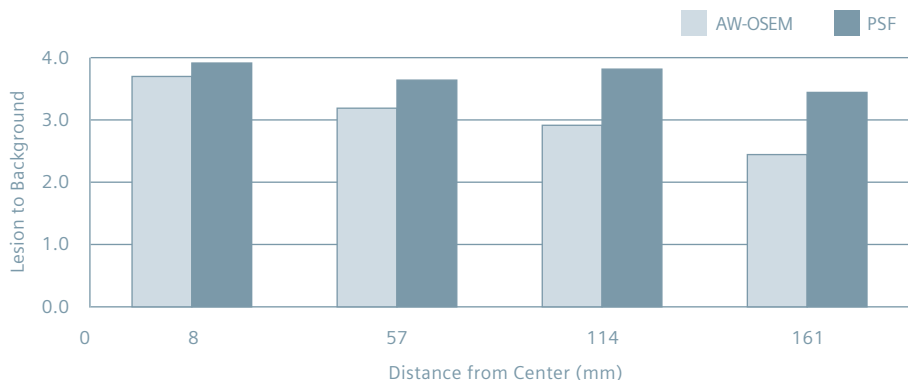


Figure 4. Lesion recovery for both AW-OSEM and PSF reconstructions.

In the NEMA standard, NU 2-2001, the image quality measurement describes a method of determining both contrast and noise of an image in a clinically relevant protocol. For this study, the phantom was filled with a four to one sphere to background ratio as described in the standard. Both the out of field of view phantoms were used as well. The phantom was imaged in a Biograph 6 TruePoint PET•CT with TrueV for 540 seconds as prescribed for a 100 cm image in 60 minutes. The images were reconstructed with both PSF and AW-OSEM in 336 x 336 images, using four iterations and 14 subsets. ROIs were drawn on the spheres and in the background according to the standard. The contrast and variability of the four hot spheres is shown in Table 1. PSF reconstruction exhibits both a greater contrast to background ratio and lower variability for all spheres when compared to the AW-OSEM.

Sphere Diameter	AW-OSEM		PSF	
	Contrast	Variability	Contrast	Variability
10	54%	11%	57%	7%
13	74%	9%	81%	6%
17	75%	7%	81%	5%
22	87%	5%	89%	4%

Table 1. Contrast and variability for the four hot spheres in the NEMA image quality phantom at the center of the field of view.

Patient Imaging

The improvements shown above in the phantom imaging are carried into clinical imaging. In one study, a 144 kilogram patient (BMI 44.2) was imaged in a Biograph 6 TruePoint PET•CT with TrueV extended field of view. The patient was injected with 10 milliCuries of ¹⁸F-FDG with a 90 minute uptake period. The scan consisted of five bed positions, covering approximately 75 centimeters in 15 minutes. The images, shown in Figure 5, were reconstructed with AW-OSEM using three iterations and eight subsets and PSF using two iterations and 14 subsets. The AW-OSEM image has been post filtered with a 6 mm Gaussian filter while the PSF was filtered with a 5 mm Gaussian.

To further illustrate the improvement obtained by the PSF reconstruction, a 51 year-old female weighing 153 pounds was injected with approximately 10 milliCuries of ¹⁸F-FDG. After a 90 minute

uptake period, data was acquired for 10 minutes. The image was reconstructed with both AW-OSEM using 4 iterations and 16 subsets and PSF with 6 iterations and 14 subsets. The AW-OSEM image was post filtered with a 5 mm three dimensional Gaussian filter. The images are shown to the right in Figure 6.

Conclusions

The introduction of AW-OSEM reconstruction into positron emission tomography brought a dramatic improvement in image quality. Now with this new reconstruction algorithm called TrueX, even better image quality can be obtained by concentrating on details such as proper treatment of the corrections and the event detection physics.

References

Shepp L. and Vardi Y.. "Maximum likelihood reconstruction for emission tomography. IEEE Transactions on Medical Imaging 1(2): 113–122. 1982

H. M. Hudson and R. S. Larkin, "Accelerated image reconstruction using ordered subsets of projection data," IEEE Trans. Med. Imag., vol.13, no. 4, pp. 601–609, Dec. 1994.

M. Defrise, P. E. Kinahan, D. W. Townsend, C. Michel, M. Sibomana, and D. F. Newport, "Exact and approximate rebinning algorithms for 3-D PET data," IEEE Trans. Med. Imag., vol. 16, no. 2, pp. 145–158, Apr. 1997.

C. Comtat, C. F. Bataille, C. Michel, J. P. Jones, M. Sibomana, L. Janeiro, and R. Trebossen, "OSEM-3-D reconstruction strategies for the ECAT HRRRT," in 2004 IEEE NSS MIC Conf. Rec., Rome, Italy, Oct. 2004, vol. 6, pp. 3492–3496.

C. C. Watson, "New, faster, image-based scatter correction for 3-D PET," IEEE Trans. Nucl. Sci., vol. 47, no. 1, pp. 1587–1594, Aug. 2000.

M. Casey, H. Gadagkar, and D. Newport, "A component based method for normalization in volume PET," in Proc. 1995 Int. Meeting Fully Three-Dimensional Image Reconstruction Radiol. Nucl. Med., pp.67–71.

Panin, V., Kehren, F., Michel, C., Casey, M., "Fully 3-D PET Reconstruction With System Matrix Derived From Point Source Measurements"; IEEE Trans Med Imaging; Vol. 25. No 7.; June 2007

NEMA Standards Publication NU 2-2001 Performance Measurements of Positron Emission Tomographs.

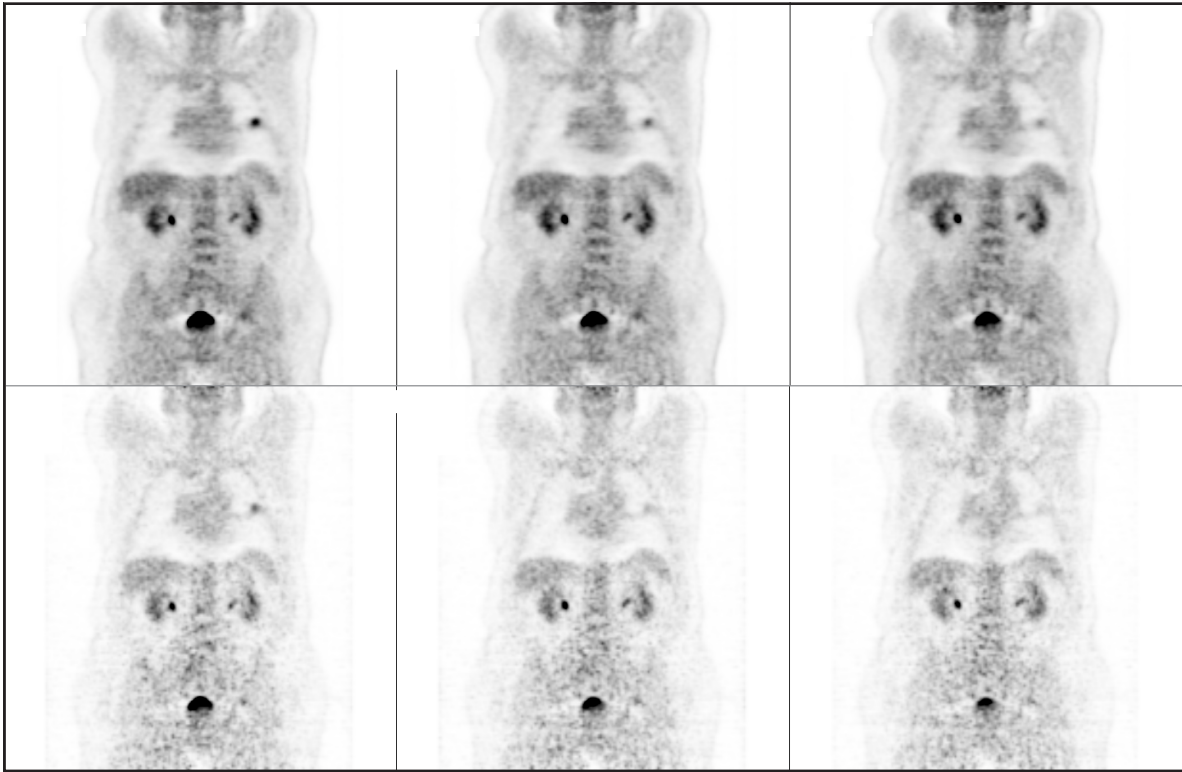


Figure 5.
144 kg patient
(BMI 44.2) imaged
for 15 minutes.

Upper:
PSF reconstruction.

Lower: AW-OSEM
reconstruction.

*Photo courtesy of
the University of
Tennessee*

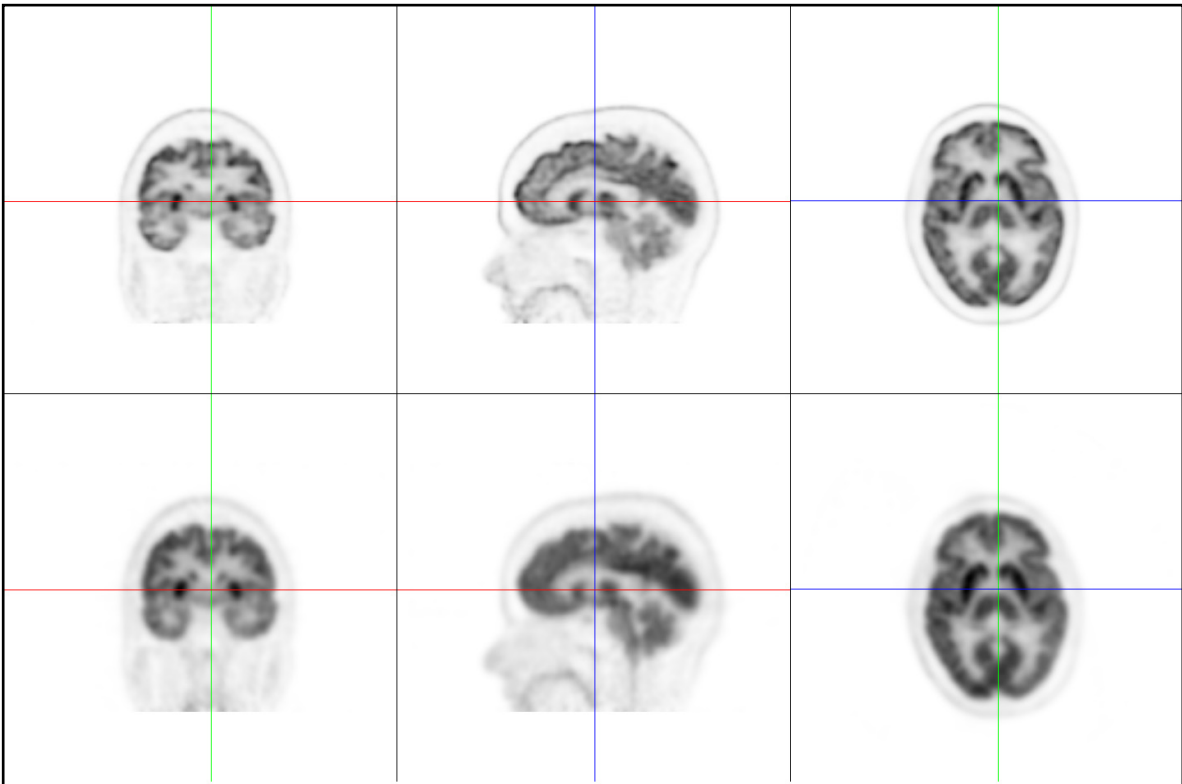


Figure 6.
153 pound patient
imaged for
10 minutes.

Upper: PSF
reconstruction.

Lower: AW-OSEM
reconstruction.

*Photo courtesy of
the University of
Tennessee.*

© 2007 Siemens Medical Solutions USA, Inc.
All rights reserved.

All photographs © 2007 Siemens Medical
Solutions, USA, Inc. All rights reserved.

Note: Original images always lose a certain
amount of detail when reproduced.

© 05.2007, Siemens AG
Order No. A91MI-10018-1T-7600
Printed in USA
PA 0507/3

Address of legal manufacturer
Siemens Medical Solutions USA
Molecular Imaging
2501 N. Barrington Road
Hoffman Estates, IL 60192-5203
USA

www.siemens.com/mi

Headquarters

Siemens Medical Solutions USA, Inc.
51 Valley Stream Parkway
Malvern, PA 19355-1406
USA
Telephone: +1-888-826-9702
www.usa.siemens.com/mi

Contact Address

Siemens Medical Solutions USA
Molecular Imaging
2501 N. Barrington Road
Hoffman Estates, IL 60192-5203
USA
Telephone: +1-888-826-9702
www.siemens.com/mi

Siemens Medical Solutions USA
Molecular Imaging
810 Innovation Drive
Knoxville, TN 37932-2751
USA
Telephone: +1-888-826-9702
www.siemens.com/mi